Moonquakes: Mechanisms and Relation to Tidal Stresses

Abstract. *Observed features of moonquakes are combined with theoretical calculations of the tidal stresses to interpret the moonquake mechanisms. Tidal stresses, together with a postulated ambient tectonic stress, are sufficient to explain the depth, periodicity, and polarity reversal of moonquakes. Both of these stresses are small (on the order of 1 bar) and consistent with the small magnitudes of moonquakes.*

A network of four seismic stations deployed on the moon during the Apollo missions has recorded more than 1000 moonquakes since 1969. These moonquakes are very small, with estimated magnitudes of less than about 2 (*1*). The annual release of seismic energy is about 10^{15} ergs, or about ten orders of magnitude less than that of the earth. Some selected moonquake epicenters and the seismic stations are shown in Fig. 1a.

Moonquakes exhibit several outstanding features. First, nearly all moonquakes, except for a small number of shallow events, occur deep inside the moon at depths of between 600 and 1000 km. Second, moonquakes occur repeatedly at distinct foci and events from each focus produce matching waveforms. So far, 68 such repeating foci have been identified. Third, the events at each focus occur at 27-day intervals. There is also evidence of a 206-day periodicity and the suggestion of a 6-year periodicity. These periodicities clearly relate the moonquake occurrences to the tidal forces acting on the moon.

Finally, we have recently found that some of the moonquakes originating at the A_1 focus, the site with the longest history and the largest number of recorded moonquakes, were of reverse polarity between 1972 and 1975 with respect to events occurring before and after this period. In other words, the direction of the motion at the source had reversed for a period of 3 years and then returned to the original direction.

In an effort to understand the above properties and the mechanisms of moonquakes, we calculated the tidal stresses in the moon, using a radially heterogeneous model based on the most recent seismic data. We then correlated the depth and time dependence of the calculated stresses with the moonquake occurrences at different foci.

For the numerical calculations, we used an approach similar to that applied on the earth. The total potential was expressed as the sum of the self-gravitational potential and the tidal potential. We calculated the tidal potential as a function of time, using Brown's theory of lunar motion (*2*). The equilibrium conditions were expressed in terms of three simultaneous differential equations, which were then solved numerically. Because the moon has no large liquid core, we obtained an asymptotic solution at a very small radius, and then propagated the solution outward by means of a rational extrapolation algorithm with a variable step size. A lunar model with a radially varying shear modulus but constant bulk modulus and density, chosen from the most recent lunar models (*3*), was used in the calculations.

The relationship between the focal depths of the moonquakes and the tidal stresses is illustrated in Fig. 1b. The calculated maximum shear stress reaches a broad high in the depth range between 600 and 900 km, closely coinciding with the moonquake depths. This shear stress high is controlled primarily by the shear modulus profile. However, any shear modulus profile consistent with the seismic data, that is, one that has a sharp drop below about 600 km, produces a maximum shear stress profile similar to that in Fig. 1b, with minor differences in the stress level and the peak. The maximum shear stress is less than 1 bar at all depths.

Calculated tidal stresses show 27-day and 206-day periodicities, arising from the monthly period of the lunar orbit and the solar perturbation of this orbit, respectively. The times of the maxima of the various stress components depend on the location in the moon. Stress components were calculated at locations corresponding to the foci of the moonquakes to be studied. The occurrence times and peak amplitudes of the moonquakes at site A_{18} are shown in Fig. 1c. This focus was active over a 3-year period, and all the events were of the same polarity. In general, there was only one moonquake per month, although occasionally two events occurred within a few days of each other in which case only the larger is plotted (Fig. 1c). Also plotted in Fig. 1c are two components of the calculated tidal stress at the same focus. The occurrence times of these moonquakes are correlated with the peaks of the stress components σ_{xy} and σ_{yy} (*x* and *y* are coordinate axes in a

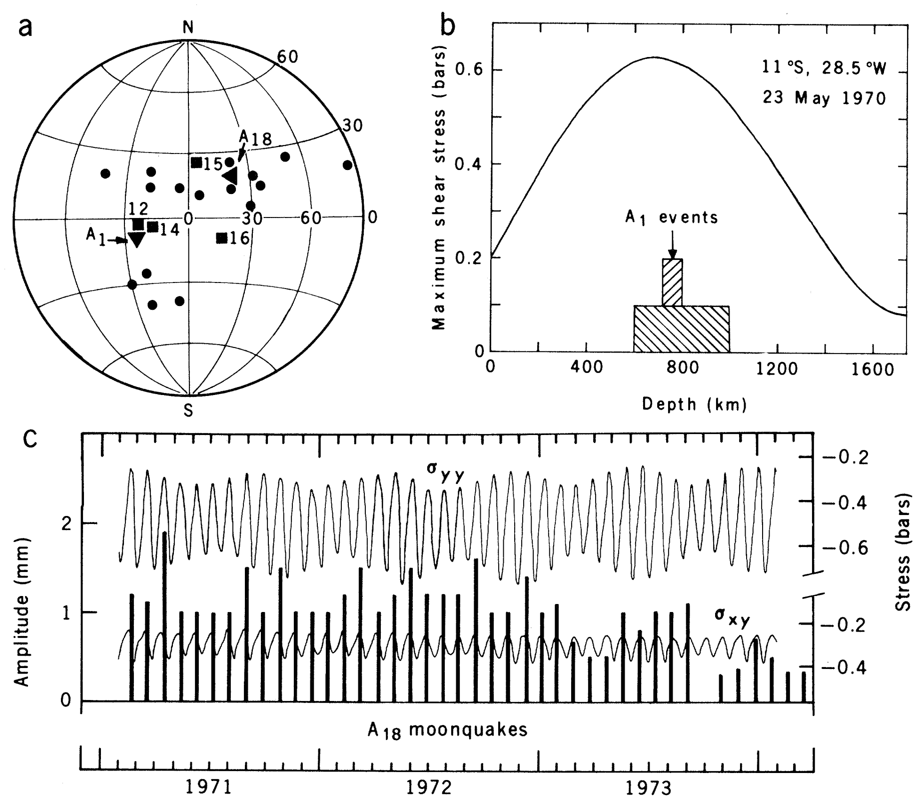

Fig. 1. (a) Locations of selected moonquake epicenters (circles) and seismic stations (squares with Apollo mission numbers). Triangles mark the locations of the A_1 and A_{18} moonquakes discussed in this report. (b) Maximum tidal shear stress as a function of depth at the A_1 location. The large box indicates the approximate depth range of the moonquake foci. The small box marks the depth of the A_1 focus. (c) History of the A_{18} moonquakes over a 3-year period. The height of each vertical bar is proportional to the maximum amplitude (on the seismogram) of the events for each month. The computed tidal stress components σ_{xy} and σ_{yy} at the A_{18} focus are also shown.

plane perpendicular to the earth-moon line, with x positive westward and y positive southward). The A_{18} moonquakes seem to occur when the normal stress σ_{yy} provides maximum unloading (least compression) on a vertical plane oriented in the east-west direction. Simultaneously, the shear stress σ_{xy} on this plane reaches an extremum at each moonquake occurrence. Other components of the stress are not correlated with the occurrence of A_{18} moonquakes. If we assume that moonquakes, like earthquakes, are caused by shear slip across a surface or a dislocation, then a vertical plane oriented in the east-west direction would be a good candidate fault plane. The correlation between the calculated tidal stresses and the observed moonquake occurrences can also explain the observed relationships between the moonquake events and the latitudinal librations of the moon, since the tidal stresses are associated with these librations (*4*). Although stresses associated with all lunar motions contribute to the occurrence of moonquakes, a particular stress component may dominate at a given focus.

An important feature of these comparisons is that, although the changes in tidal stresses are small, they seem to be adequate to generate small moonquakes. A similar correlation of some small earthquakes and earthquake swarms with tidal stresses has been observed (*5*). Although the much larger tectonic stresses control most earthquake occurrences, the relatively rapid rate of stress changes associated with the semidiurnal tides may be the cause of some earthquake swarms (*5*).

It is also important to examine the moonquakes that show polarity reversals. We examined the time history of the moonquake occurrences and reversals over a 6-year period at the A_1 focus (Fig. 2a). In Fig. 2b, the three stress components and the moonquakes are shown for three different time periods: the first in 1970 during a period of normal polarity, the second in 1973 characterized by reversed events, and the third in the subsequent normal period in 1975; x and y here have the same meaning as in Fig. 1c, and the component σ_{zz} is in the direction of the earth-moon axis (positive toward the earth). The most obvious result from this comparison is that all A_1 moonquakes, both normal and reversed, occur at maxima of σ_{zz}, when the tidal pull toward the earth is strongest. As in the case of the A_{18} focus, this result suggests that a plane oriented perpendicular to the earth-moon axis would be a likely fault plane and that all A_1 moonquakes occur when the tidal unloading allows slippage on this plane.

The calculated tidal stresses (Fig. 2b) do not show a sign reversal of any stress component over the 6-year period and cannot account for reversals in moonquake polarity. The reversals can be explained, however, if there is an ambient stress of constant direction and magnitude, adding a bias to the oscillating tidal stresses. The resultant stress (tidal plus ambient) changes the direction of the slip, as shown in Fig. 2c, if the magnitude of the ambient stress is between the minimum and maximum of the tidal stresses. In fact, the reversals can be fitted consistently with an ambient stress of about 0.5 bar. This ambient stress could be due to tectonic forces frozen in the lunar mantle or to convection deep in the lunar interior. The small magnitude of the stresses is in agreement with the low seismicity of the moon. The occasional near-surface moonquakes, which are not correlated with the tides, are probably due to the release at random times of the tectonic stresses frozen in the lunar crust, and they may resemble terrestrial intraplate earthquakes.

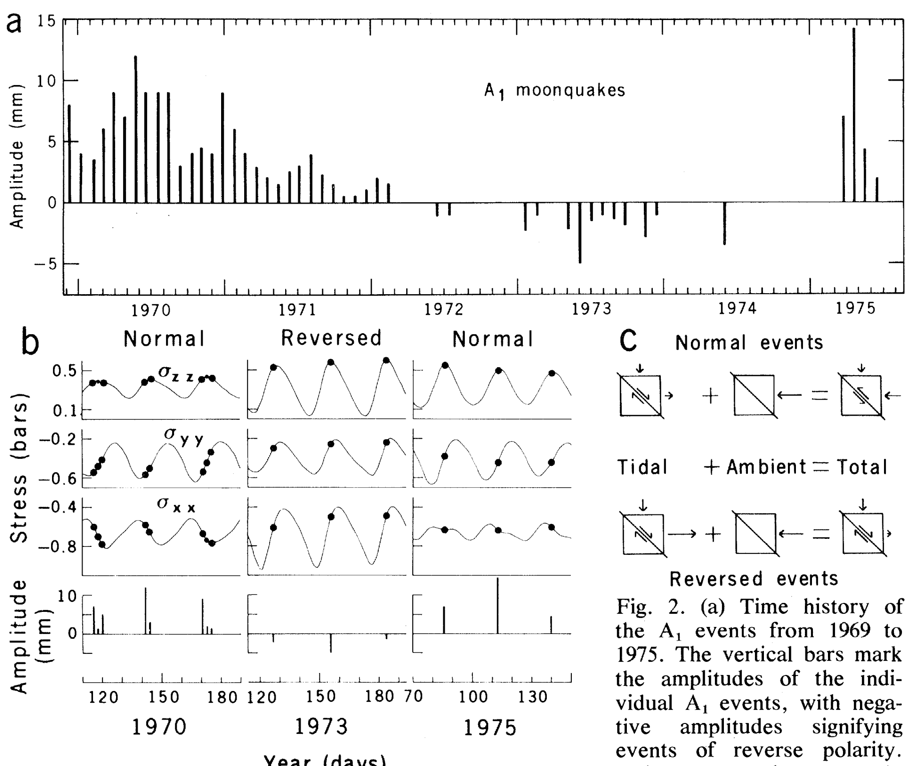

Fig. 2. (a) Time history of the A_1 events from 1969 to 1975. The vertical bars mark the amplitudes of the individual A_1 events, with negative amplitudes signifying events of reverse polarity. (When more than one A_1 event occurred within a few days, only the largest has been plotted.) (b) Tidal stress components plotted as a function of time for three representative periods: the period of normal polarity in 1970, the period of reverse polarity in 1973, and the normal period in 1975. The A_1 moonquake occurrences are marked both by bars on the amplitude curve and by dots on the stress curves. (c) A schematic diagram showing the interaction between the cyclic tidal stresses and a constant ambient tectonic stress to produce normal and reverse moonquakes. The stress components due to tides (first column) oscillate in magnitude but do not reverse direction and therefore cannot produce a reversal of polarity. The addition of a constant, ambient tectonic stress (second column) in each case could produce a reversal, as shown in the third column.

The following conclusions can be derived from the comparison of the calculated tidal stresses and the characteristics of moonquake occurrences:

1) Most moonquakes occur at depths where tidal shear stresses are at a maximum. This depth depends on the shear modulus profile inside the moon. Thus, the focal depths of the moonquakes are determined by both the elastic properties of the lunar interior and the tidal stresses.

2) The occurrence times of moonquakes are strongly correlated with the maxima of some component of the tidal stress at that site. If moonquakes are associated with weak zones or faults in the lunar interior, then the tidal stress component acting on this plane would be the controlling factor in the occurrence of moonquakes.

3) The polarity reversal of the A_1 moonquakes, and thus the reversal of slip motion at the A_1 source, can be explained in terms of a combination of the cyclic tidal stresses and a constant, ambient tectonic stress. The magnitude of the required tectonic stress is about 0.5 bar, whereas the tidal stresses are on the order of 1 bar. These small stresses are consistent with the low seismicity of the

moon, and they suggest that any convection inside the moon is most likely weak and cannot induce large stresses in the lunar lithosphere.

M. NAFI TOKSÖZ
NEAL R. GOINS, C. H. CHENG
Department of Earth and Planetary Sciences, Massachusetts Institute of Technology, Cambridge 02139

References and Notes

1. D. R. Lammlein, G. V. Latham, J. Dorman, Y. Nakamura, M. Ewing, *Rev. Geophys. Space Phys.* **12**, 1 (1974); G. Latham, M. Ewing, J. Dorman, D. Lammlein, F. Press, N. Toksöz, G. Sutton, F. Duennebier, Y. Nakamura, *Science* **174**, 687 (1971); Y. Nakamura, J. Dorman, F. Duennebier, M. Ewing, D. Lammlein, G. Latham, *Geochim. Cosmochim. Acta* 3 (Suppl. 5), 2883 (1974).
2. A. E. H. Love, *Some Problems of Geodynamics* (Dover, New York, 1967), p. 180; H. Takeuchi, *Trans. Am. Geophys. Union* **31**, 651 (1950); J. C. Harrison, *J. Geophys. Res.* **68**, 4269 (1963); W. M. Kaula, *ibid.*, p. 4959. The equation for Brown's theory can be found in the *Explanatory Supplement to the Astronomical Ephemeris and the American Ephemeris and Nautical Almanac* (Her Majesty's Stationery Office, London, 1961).
3. M. N. Toksöz *et al.*, *Rev. Geophys. Space Phys.* **12**, 539 (1974); A. M. Dainty, N. R. Goins, M. N. Toksöz, *Geochim. Cosmochim. Acta* 3 (Suppl. 6), 2887 (1975); A. M. Dainty and M. N. Toksöz, *Geochim. Cosmochim. Acta* (Suppl. 7), in press; Y. Nakamura, G. Latham, D. Lammlein, M. Ewing, F. Duennebier, J. Dorman, *Geophys. Res. Lett.* **1**, 137 (1974).
4. D. R. Lammlein, *Geochim. Cosmochim. Acta* (Suppl. 7), in press; R. Meissner, J. Voss, H. J. Kaestle, *Moon* **6**, 292 (1973).
5. T. H. Heaton, *Geophys. J. R. Astron. Soc.* **43**, 307 (1975); F. W. Klein, *ibid.* **45**, 245 (1976).
6. Moonquake catalogs used in this study were prepared at the University of Texas (Galveston) by Drs. G. Latham, J. Dorman, D. Lammlein, F. Duennebier, and Y. Nakamura. We thank Dr. Nakamura for many valuable suggestions at various stages of this work. This research was supported under NASA contract NAS9-12334 and grant NSG-7081.

23 August 1976; revised 23 November 1976

Nitrogen Budget for an Aggrading Northern Hardwood Forest Ecosystem

Abstract. *Long-term analyses of the structure and function of a northern hardwood ecosystem have resulted in measurement of the salient features of the nitrogen cycle. These data allow an evaluation of the importance of the various components and provide a framework for more efficient forest management.*

Nitrogen is one of the most important limiting nutrients for ecosystem production. Only now is it becoming apparent that our finite energy resources may serve as a limit for the widespread and often indiscriminate application of nitrogenous fertilizer, which was commonplace in the recent past. This realization has led to a more careful consideration of the nitrogen cycle in natural ecosystems, for it is apparent that before we can use natural sources of nitrogen more efficiently or learn how to add nitrogenous fertilizer more effectively, we must understand the nitrogen cycle in nature. Thus, the biogeochemistry of nitrogen is becoming one of the most intensively studied aspects of ecology.

Measurement of the nitrogen cycle is no small task. It requires sophisticated techniques, a well-designed model for identifying gaps, and years of careful and perceptive measurement. The data and deductions presented in this report represent the distillation of 13 years of work—literally thousands of chemical analyses of precipitation and stream water and of plant and animal tissue. For more than a decade, researchers at the Hubbard Brook Experimental Forest in the White Mountains of New Hampshire have been working to quantify the structure and function of various terrestrial and aquatic ecosystems and to determine the relationships between forested watershed ecosystems and the larger biogeochemical cycles of the earth (*1*).

A model was developed for these deciduous, northern hardwood ecosystems to facilitate the collection, analysis, and interpretation of diverse field data (*1*). Utilizing this model and the small watershed technique, it was possible to measure input and output of chemicals and water and to construct quantitative nutrient budgets for natural ecosystems. Six small drainage areas tributary to Hubbard Brook were the watershed ecosystems chosen for study (*1*). This report presents our current understanding of the nitrogen budget (Fig. 1) for one of these forested watershed ecosystems, watershed 6.

The forest on watershed 6 is about 55 years old and is dominated by sugar maple (*Acer saccharum* Marsh.), American beech (*Fagus grandifolia* Ehrh.), and yellow birch (*Betula alleghaniensis* Britt.) (*2*). The mean basal area of the forest is 24 m^2/ha, net primary production is 1040 g (dry weight) per square meter per year, and living and dead biomass accumulation is 393 g m^{-2} $year^{-1}$ (*3, 4*). The ecosystem is thus aggrading, with an annual net accumulation of biomass.

The area of watershed 6 is 13.2 ha. Climate is generally humid-continental with short, cool summers and long, cold winters. Precipitation averages about 130 cm/year and is distributed evenly throughout the year. A deep snowpack is characteristic of wintertime and soil frost is uncommon. Streamflow averages about 80 cm/year, with about 54 percent of the annual streamflow occurring during the months of March, April, and May as the snowpack melts. Bedrock and till are derived from the granitic Littleton and Kinsman formations. The thin, acidic soils are mostly well-drained podzols (haplorthods) with a thick (3 to 15 cm) organic layer at the surface. Detailed information on topography, geology, soils, hydrology, and climatic conditions have been reported elsewhere (*1, 5, 6*).

The pattern of nitrogen accumulation and transfer within the aggrading ecosystem (*7–14*) is of particular interest since it may be severely altered by disturbance (for example, clear-cutting). Understanding the pattern is thus vital to facilitating recovery processes after cutting. Several important features of the nitrogen cycle emerge from an analysis of the overall pattern (Fig. 1), and these are in general agreement with those reported for other deciduous forest ecosystems (*15, 16*).

1) Natural forested ecosystems tend to accumulate and cycle large amounts of nitrogen (*1, 6, 17*).

2) Some 68 percent of the nitrogen that is added to the ecosystem each year is from nitrogen fixation. Thirty-two percent is added in bulk precipitation, and little, if any, is added by weathering.

3) Of the estimated 20.7 kg/ha entering the system each year, about 81 percent is held or accreted within the ecosystem.

4) Of the 83.5 kg/ha added to the inorganic pool within the ecosystem, only a small fraction, 5 percent, leaks out of the system in streamflow.

5) Of the 119 kg of nitrogen estimated to be used in growth processes by plants, 33 percent is withdrawn from storage locations within the living plants in the spring and utilized in growth, and a like amount is withdrawn from the leaves and stored in more permanent tissues shortly before leaf senescence in the autumn.

6) Of the nitrogen accreted into long-term storage, some 54 percent is added to living biomass, while 46 percent is stored in organic matter of the forest floor.

7) Root exudation, for the first time quantitatively estimated for an entire ecosystem, releases about 1 percent of the inorganic nitrogen made available by net mineralization.

8) Most of the nitrogen in a northern hardwood forest ecosystem, approximately 90 percent, is in soil organic matter; about 0.5 percent exists as available